Journal Pre-proofs

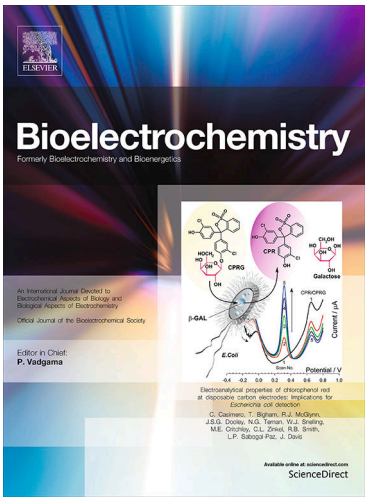

Ultrasensitive detection of MicroRNA-21 by using specific interaction of antimonene with RNA as electrochemical biosensor

Ya Zhang, Ning Li, Wenhao Ma, Mei Yang, Faliang Xu, Changjun Hou, Danqun Huo

PII: S1567-5394(21)00153-5
DOI: https://doi.org/10.1016/j.bioelechem.2021.107890
Reference: BIOJEC 107890

To appear in: *Bioelectrochemistry*

Received Date: 4 July 2021
Accepted Date: 13 July 2021

Please cite this article as: Y. Zhang, N. Li, W. Ma, M. Yang, F. Xu, C. Hou, D. Huo, Ultrasensitive detection of MicroRNA-21 by using specific interaction of antimonene with RNA as electrochemical biosensor, *Bioelectrochemistry* (2021), doi: https://doi.org/10.1016/j.bioelechem.2021.107890

This is a PDF file of an article that has undergone enhancements after acceptance, such as the addition of a cover page and metadata, and formatting for readability, but it is not yet the definitive version of record. This version will undergo additional copyediting, typesetting and review before it is published in its final form, but we are providing this version to give early visibility of the article. Please note that, during the production process, errors may be discovered which could affect the content, and all legal disclaimers that apply to the journal pertain.

© 2021 Published by Elsevier B.V.

Ultrasensitive detection of MicroRNA-21 by using specific interaction of antimonene with RNA as electrochemical biosensor

Ya Zhang[1,a], Ning Li[1,a], Wenhao Ma[a]， Mei Yang[a], Faliang Xu[a,b], Changjun Hou[a,*], Danqun Huo[a,c,*]

a Key Laboratory for Biorheological Science and Technology of Ministry of Education, State and Local Joint Engineering Laboratory for Vascular Implants, Bioengineering College of Chongqing University, Chongqing g 400044, PR China
b Treatment Center of Breast Diseases, Chongqing Cancer Institute and Hospital, Chongqing University, Chongqing 400030, PR China c Chongqing Key Laboratory of Bio-perception & Intelligent Information Processing, School of Microelectronics and Communication Engineering, Chongqing University, Chongqing, 400044, PR China
* Corresponding author. Tel.: +86 23 6511 2673; fax: +86 23 6510 2507.
E-mail addresses: huodq@cqu.edu.cn (D. Huo)
houcj@cqu.edu.cn (C. Hou)

1. Using specific interaction of antimonene with RNA as an electrochemical biosensor.
2. The ssRNA can adsorb on the antimonene.
3. The dsRNA easily desorbed from the antimonene interface

Abstract

Journal Pre-proofs

MicroRNA exhibits different levels of expression in cancer and can affect the transformation, metastasis, and carcinogenesis of the cancer cell. Herein, we developed a novel kind of electrochemical microRNA biosensor based on two-dimensional nanomaterial of antimonene nano-flakes (AMNFs) and carbon quantum dots (CQDs) which were used as substrating to cadmium ion (Cd^{2+}) for specific detection of breast cancer-relevant biomarker-microRNA-21. Compared to graphene, the first principle energetic calculation shows that the AMNFs have completely a stronger force interaction with single strand (ssRNA), due to the antimonene has a more delocalized 5s/5p orbital.

After the addition of complementary microRNA, due to the low adsorption affinity of double-stranded RNA (dsRNA) to antimonene, the hybridized target is easy to desorb from the antimonene interface, and the oxidation peak of metal ions is significantly reduced. Results showed the microRNA-21 concentration can be detected from 100 aM to 1 nM, the limit of detection as low as 21 aM toward microRNA-21, which is 3 times lower than those of the established microRNA biosensors. The unique combination of not be attempted before existing sensing material which has special adsorption properties represents an approach to the detection of breast cancer. And it provides a promising method for early diagnosis, monitoring, and staging of breast cancer.

Keywords: Electrochemical microRNA biosensor, Breast cancer, AMNFs, Carbon quantum dots, Cadmium ion, MicroRNA-21

1. Introduction

Now, there is a growing number of diseases, in particular, it is known that cancer as a cause of death, especially breast cancer, is one of the most common malignancies in the world. And the key to its early diagnosis is that low cost, easy, high potential, and easy treatment [1]. The early detection of tumor biomarkers has potential in the diagnosis, prediction, and monitoring of disease.

MicroRNA, a short single strand of ribonucleic acid (RNA) molecule typically

consists of 19 to 23 nucleotides, is a candidate non-invasive biomarker for application in diagnosis, adverse event, and toxicology or monitoring treatment responses [2,3]. The microRNA-21, is an important circulating and robust oncogenic microRNA, involve in the carcinogenic process, and it serves as a biomarker for diagnosis, progression, staging, and prognosis of breast cancer [4,5]. Furthermore, the microRNA -21 is very stable in human serum, so its sampling is non-invasive and easy to extract [8]. In addition, it is also used as a biomarker for diagnosing early breast cancer, it is highly conserved, time-series, tissue specificity, and over-expression during the process of cancer [6,7]. At the represent, the traditional way to detect microRNAs by some molecule detection methods such as Northern blotting, real-time quantitative polymerase (qRT-PCR) and microarray analysis, however, they are very laborious, costly, the difficulty in amplification and low sensitivity [8,9].

In recently, the booming of electrochemical nanosensors has enabled us to see more rapid, simple, effective, and low-cost methods for disease diagnosis [10]. Electrochemical nano biosensors combine with the advantages of the electrochemical biosensor with nanotechnology, reliable, easy-to-use, has resulted in generating a new type of low cost and ultrasensitive diagnostics [11,12]. Nanomaterials own unique physicochemical characteristics, which offer desirable and unmatched properties such as strong signal intensities, big surface area, and can finely adjust the surface chemistries for detection [13,14]. To date, there are some nanomaterials such as quantum dots, carbon nanotubes, Au nanoparticles, and so on, that have been used to sensitivity diagnostic cancer for biomarkers in vitro [15,16]. Among them, due to their excellent hydrophobicity, easy synthesis, electro-conductivity, biocompatibility, chemical stability, cost efficiency, and properties, CQDs can be used as an ideal electrochemical platform [17,18]. Although many biosensors simply are dropped nanomaterials onto their surfaces of electrodes, the adsorption can not be stable on the surface [19,20]. The number of biomolecules bound to the nanoparticles is reduced due to the random arrangement of nanoparticles blocking many active sites. Thus, there is an urgent need to find good absorbent and stable material in a particular area of electrode to increase the sensitivity of biomarker detection [21,22].

Nowadays, antimonene is one of the most popular two-dimensional atomic semiconductor materials, which can change its physical properties such as molecular recognition and band-gap modulation due to its ability to undergo non-covalent binding of the recipient [23]. Therefore, its application will be very promising in the field of biosensors. Antimonene can be separated from powdered antimony (Sb), and its physical and chemical properties exceed the superior properties of two-dimensional materials, which has rapidly attracted wide attention in the scientific community [24]. Similar to graphene materials, antimonide has an sp^2-bonded honeycomb lattice, but antimonene shows significantly better spin-orbit coupling, great stability, and hydrophilicity than graphene. Antimonene nanosheets and their quantum dots have been used in nonlinear optics, thermo-optoelectronics (TPV), photothermal therapy (PTT), batteries, and field-effect transistors (FET)[25]. Although the photoelectric properties of antimonene have also been studied. The interaction between RNA and antimonene which its application has not been explored in the field of electrochemical sensing.

As a new kind of super-sensitive two-dimensional material, antimonene especially has the function of non-covalent binding with some biomaterials, so it can be used for molecular recognition. In addition, according to the first-principles density functional theory (DFT) calculations, the antimonene has a special chemical interaction with single ssRNA and dsRNA) [26,27]. This is due to the strong interaction between ssRNA and antimonene and the adsorption on the antimonene nanosheets. After the addition of complementary microRNAs, due to the low affinity between dsRNA and antimonene, the hybridization target is easy to desorption from the antimonene interface. Based on this discovery, we developed an electrochemical microRNA biosensor that used AMNFs for trace quantification of microRNA-21 molecules. We have prepared AMNFs coupling with CQDs (represented by ssRNA-CQDs-Cd^{2+}/AMNFs) and explored it as the platform for anchoring microRNA (Scheme 1). Combining the advantages of a large specific area, strong affinity, high stability, excellent biocompatibility of antimonene and high electrochemical activity, and outstanding biosensing performance of CQDs, the fabricated ssRNA-CQDs-

Cd^{2+}/AMNFs-based electrochemical microRNA biosensor can be applied to sensitively detect the trace microRNA-21 in a human serum sample. The electrochemical ssRNA-CQDs-Cd^{2+}/AMNFs based biosensor displays extremely low limitations of detection (LOD) toward microRNA-21, also with good stability, selectivity, reproducibility, and acceptable applicability.

As far as we know, although there are few works in the literature about AMNFs aimed at detecting ssRNA alterations by fluorescent microscopy or fluorescence resonance energy transfer, this is the first time that the AMNFs are employed to develop a very selective electrochemical microRNA biosensor. This microRNA sensing device can be used for early cancer diagnosis and further clinical applications.

2. Experimental section

2.1 Materials and reagents

Antimony powder from Smart Elements (99.999% purity), ethanol, citric acid, metal ion, N-hydroxysuccinimide (NHS), N-methyl pyrrolidone (NMP), 1-ethyl-3-(3-dimethyl aminopropyl) carbodiimide hydrochloride (EDC). All chemicals were purchased from Aladdin (Shanghai, China). Synthetic the capture probe-ssRNA and microRNA oligonucleotides sequences were provided by Sangon Biotech Co, Ltd (Shanghai, China). The phosphate buffer solution for ssRNA absorbed was 10 mM K_2HPO_4 containing 1.0 M NaCl (pH 7.0). Human serum samples used for labeled recovery of microRNA 21 were obtained from Baoguang Biotechnology.

Probe ss-RNA：5’-NH_2-UCA ACA UCA GUC UGA UAA GCU A-3’

Target microRNA-21：5’-UAG CUU AUC AGA CUG AUG UUG A-3’

Non-complementary microRNA：5’-ACC GCA CAG GUG GAA UCU AAC G- 3’

Bases mismatch target: 5’-UAC CUG AUC GGA CUU GUG GUG A- 3’

2.2 Characterizations.

Chongqing Graduate Tutor Team Construction Projectandand， Analytical and Testing Center of Chongqing University for Infrared spectra were recorded with a Nico-let 6700 FT-IR spectrophotometer (Madison, Wisconsin, USA). The transmission electron microscopy (TEM) , X-ray photoelectron spectroscopy (XPS),

diffraction of x-rays (XRD) and atomic force microscope (AFM), respectively.) and the sharing fund of Chongqing University's large equipment.

2.2 Preparation of AMNFs

AMNFs were prepared by using the probe ultrasonic method in NMP by liquid phase stripping breaking weak van der Waals force[28]. Antimony (Sb) powder with an initial concentration of 30 mg mL^{-1} was dispersed in glass bottles containing NMP. Then, Sb powder solution was ultrasonicated in a 450 W, 22 kHz ice bath for 1 h with a 0.5 s pulse ultrasonic probe. After that, centrifuge the resulting solution at 150.3 ×g for 10 minutes. The nanosheets containing antimonene are carefully collected overnight in a clean test tube for future use.

2.3 Preparation of CQDs

The CQDs were synthesized by hydrothermal synthesis reported by a hydrothermal method [34]. An appropriate amount of citric acid was weighed, ground into powder in an agate mortar, and then poured into the Teflon-lined stainless autoclaves at 200 ℃ for 3 h to yield CQDs. After cooling, the yellow liquid was obtained. The product was moved into a 50 mL centrifuge tube, added water to the line, isolated for 10 min at 5000 r/min, and the supernatant was placed in a 4 ℃ refrigerator for standby use.

2.4 Preparation of CQDs-Cd^{2+}

In this study, cadmium ion can also be adsorbed on CQDs as signals of electrochemical detection. To synthesize biocides, 2 mL CQDs have dispersed in 2 mL of 10 mg/L $Cd(NO_3)_2.4H_2O$ solution and keep shaking at room temperature for 24 h. The mixed solution was dialyzed using a 1 kDa dialysis bag to remove unadsorbed $Cd(NO_3)_2$. The stock solution of CQDs-Cd^{2+} in 0.1 M phosphate buffer saline (PBS, pH 7.4) was stored at 4 ℃.

2.5 Preparation of CQDs-Cd^{2+}-ssRNA

In this study, CQDs were easily bonded with the amino group using EDC/NHS covalent chemistry [35]. In brief, firstly, 0.1 M EDC was mixed with 2 mL CQDs solution (in phosphate-buffer saline (PBS)), and EDC reacted with the carboxyl group of CQDs to create an active-easter intermediate within 30 min of shaking at room temperature. Then, 0.1 M NHS and 1 mL of ssRNAs were added to enable an amine reaction between an amino group and the end of ssRNAs and keep shaking continuously at 7 ℃ for 16 h. The reaction solution was dialyzed using a 1 kDa dialysis bag to remove unreactive EDC and NHS. Finally, the reaction solution of ssRNA-conjugated CQDs in 0.1 M phosphate buffer saline (PBS pH 7.0) was store at 4 ℃.

2.6 Preparation of electrochemical biosensor for microRNA-21

Initially, before use, the cleaning of GCE was conducted. The GCE was polished with a 0.05 μm and 1.0 μm alumina powder to slurry on a smooth polishing cloth and cleaned by ultrasounds for 1 min in ethanol and water until a mirror-like surface was obtained. Then, rinsed thoroughly with deionized water and dry with an ultra-pure nitrogen flow. Secondly, dropped AMNFs onto clean bare GCE and let dry naturally at room temperature for 1 h. After that, AMNFs modified GCE (AMNFs /GCE) was immersed in 200 μL immobilized PBS (pH 7.0) containing 1.0 μM ssRNA-Cd^{2+}-CQDs and adsorbed at 0 ℃ for 30 min. After being adsorption, and the unbound ssRNA was removed with PBS, followed by the resulting electrode (ssRNA-Cd^{2+}-CQDs-AMNFs/GCE), the ssRNA immobilized electrodes were incubated into target microRNA-21 for 60 min to achieve hybridization (microRNA/ssRNA-Cd^{2+}-CQDs-AMNFs/GCE). Finally, the oxidation current of Cd^{2+} was measured by SWV in PBS (pH 7.4).

First, metal ions and CQDs were applied to connect with ssRNA to enlarged the electrochemical signal. Then, the ssRNA-Cd^{2+}-CQDs-enlarged complex was adsorbed onto AMNFs. After the addition of complementary microRNA-21, due to the low affinity between dsRNA and AMNFs, the hybrid target was easily desorbed from the AMNFs interface. The amount of microRNA-21 can be typically determined based on

the electrochemical signal of SWV. The entire detection process, including each modification step of each electrode, required a time of 2.5 h. The electrochemical signal of Cd^{2+} was determined from -1.0 V to -0.4 V before and after hybridization, it turned out that the significant reduction in peak current was attributable to the target microRNA-21 concentration. The construction and detection strategy of the electrochemical microRNA-21 biosensor was illustrated in Scheme 1.

3. Results and discussions

3.1 Characterization of AMNFs and CQDs

Antimonide suspensions have been prepared by probe sonication-assisted exfoliation in NMP. After centrifugation, we have achieved the final concentration and homogeneity of the AMNFs suspension, which is on an order of magnitude similar to those already reported. In the TEM image shown in Fig 1A, the AMNFs have a smooth surface and large surface area. The microstructure of the CQDs was inspected by TEM, and the images are shown in Fig 1B. The sample showed the average size of the CQDs was 1 nm. The AFM topography of typical antimonene nanosheets is shown in Fig 1C. The overall lateral dimensions of the nanosheets are greater than 400 nm, and the thickness of the thinnest sheet is about 3 nm.

XRD spectrum of AMNFs as shown in Fig 2A, the crystalline phase of AMNFs was further determined by ultrasound. The diffraction peaks of the bulk antimony-phase lattice are the same as the XRD spectra of the structure exfoliated antimony. The main peaks of AMNFs on (003), (012), (110), and (202) crystal planes overlap with the bulk sb crystal planes. Fig 2B is Fourier transform infrared spectrum, and the vibration absorption peak of CQDs after carbonization. Figure 2B shows the Fourier transform infrared spectrum. It can be seen from the spectrum (black line) that the absorption peaks of the carbonized CQDs at 1,713 cm^{-1} and 1,384 cm^{-1} are attributed to the symmetric and asymmetric stretching vibrations of the carboxylate C=O, and the peak at 911 cm^{-1} is attributed to the non-plane swinging vibration of O-H. The infrared spectrum of the amide bond formed by CQDs and aptamer chains modified by EDC and NHS, respectively, is shown in the figure (red line). The peak at 3700

cm^{-1} is the stretching vibration of the amide bond N-H, and the absorption peak at 1634.8 cm^{-1} is the symmetric stretching vibration of the amide bond C=O.

The XPS spectrum of CQDs-Cd(Ⅱ) is shown in the Fig 2C-F, where (C) is the total XPS spectrum, and (D)~(F) are the elemental peak spectra. From the XPS total spectrum (Fig (2C)) and the Cd peak (Fig (2D)), it can be seen that the Cd(3d) peak appears in the CQDs-Cd(Ⅱ) graph, indicating that the CQDs successfully adsorbed Cd.

3.2 Principle of the electrochemical microRNA biosensor

In this study, the capture probe was ssRNA, a perfectly matched complementary target microRNA-21 hybridized by hydrogen bonding. Compared with the dsRNA hybridization, the ssRNA of the hybridization molecule has greater stability. First-principles calculations (DFT) based energetic calculations including dispersive Van der Waals forces were performed to investigate the differential interactions of ssDNA and dsDNA with antimonene. The adsorption energies (Ead) of the bases on antimonene are higher than those of the base-pairs on antimonene, indicating the stronger interaction between the nucleobases and antimonene. The work function (ΔW) shows substantial increase after DNA absorption. Distinctly and importantly, we found that by comparison with graphene, antimonene exhibits the much stronger interaction with ssDNA. This is further supported by the charge density difference map between antimonene with DNA absorption and noninteracting counterparts, where the stronger charge transfer and electronic orbital hybridization occurs in the antimonene case[].

In order to investigate the hybridization efficiency of hybridization between the microRNA-21 probe and target microRNA sequence, metal ion (Cd^{2+}) was used as the signal source and electrochemical signal amplification indicator, because it can provide a well-defined square wave voltammetric (SWV) signal.

To fabricate the ssRNA-based biocides, it's important to use some suitable substrate to label ssRNA and load enough metal ions for signal development and amplification. Due to the excellent electrical conductivity, various grafting groups

(e.g -NH_2 or -COOH), and adsorption characteristics the CQDs are ideal candidates, which may facilitate the immobilization of metal ion and biological ligands. In particular, the CQDs with strong electrical conductivity and the larger specific area are suitable for the assembly of biocides. To further prove the signal of metal ions and electrochemical amplification and the CQDs modified microRNA complex is effective, each step of the modified electrodes was investigated by SWV experiments. As shown in Fig 3 (curve a), there was a significantly higher oxidation peak of metal ions on the ssRNA complex modified GCE. With the addition of complementary microRNAs, due to the low affinity of dsRNA to antimonide, the hybridization target was easy to desorb from the antimonide interface, and the oxidation peak of metal ions was significantly reduced Fig 3 (curve b).

3.3 Characterization of microRNA biosensor fabrication

To investigate the characterized of the stepwise assembly of CV and EIS was performed (Fig 4A and B). Fig 4A showed the CV results of different modified electrodes in a solution of 0.5 mM $Fe(CN)_6^{4-/3-}$ containing 0.1M KCl. Compared with bare GCE showed curve a, AMNFs modified GCE electrode has a higher $Fe(CN)_6^{4-/3-}$ current oxidation peak (Curve B), which can enhance electron transfer because the antimonene was conductive. After that, the ssRNA-Cd^{2+}-CQDs complex was self-assembled onto the surface of antimonene/GCE, the current oxidation peak of $Fe(CN)_6^{4-/3-}$ showed an obvious increase (curve c), when the AMNFs/GCE immersed in 2 mM ssRNA-Cd^{2+}-CQDs solution, due to the metal ions (Cd^{2+}) absorbed on the CQDs to increased electrical conductivity. Finally, the ssRNA-Cd^{2+}-CQDs/AMNFs/GCE immersed in 50 fM target microRNA-21, the current voltammogram oxidation peak of $Fe(CN)_6^{4-/3-}$ decreased (curve d). That can be ascribed to successfully target the microRNA-21.

Fig 4B showed the Nyquist graph impedance spectrum response of the EIS results of the modified electrode. After modification of the GCE electrode with AMNFs, the Nyquist diagram showed a distinct semicircle region (Curve b). When the AMNFs/GCE absorbed the ssRNA-Cd^{2+}-CQDs, showing a lower Ret than the

antimony/GCE. And it was a clear display that the diameter of semicircles successively decreased with the metal ions (Cd^{2+}) and CQDs (curve c), exhibiting a gradual enhancement in Ret. Subsequently, due to microRNA-21 (d), there was a significant increase in the semicircle area, indicating successful targeting of microRNA-21. These results demonstrated that were in good consistent with those of the characterization in CVs, which determined the successful construction of the microRNA biosensor.

3.4 Optimization of experimental conditions

To achieve optimal detection efficiency, the key issue of microRNA biosensors is incubation time and concentrations of ssRNA-Cd^{2+}-CQDs. The prepared electrode adsorbs different concentrations of ssRNA-Cd^{2+}-CQDs. The electrochemical signal of cadmium ions is used to prove the adsorption density of antimony on ssRNA-Cd^{2+}-CQDs. Fig 5B presents that, with incubation time increase, SWV peak current decrease. After 100 pM, the current signal nearly reached a plateau. Therefore, 100 pM was evaluated as the optimal concentration of ssRNA-Cd^{2+}-CQDs for targeting microRNA-21.

The capture time of microRNA was chosen for optimum analytical performance. The ssRNA-Cd^{2+}-CQDs/AMNFs/GCE was incubated with 40 fM microRNA solution for 20, 40, 60, 80, and 120 min, respectively. Fig 5A presents that, with incubation time increase, SWV peak current decrease. After 60 minutes, the current signal nearly reached a plateau. Therefore, 60 min was evaluated as the optimal incubation time for targeting microRNA-21.

3.5 Performance of the biosensor

Under optimal parameters, SWV revealed different electrochemical signals of Cd^{2+}， the probes were captured via ssRNA with microRNA-21 targets (Fig 6A). The peak current signal was attributed to oxidation of Cd^{2+} on ssRNA-Cd^{2+}-CQDs-AMNFs/GCE. The logarithm of the target microRNA-21 concentration showed an ideal linear ratio.

The oxidation peak current signal decreased with the increase of microRNA

from 0 pg/mL to 1000 pg/mL and SWV peak current (Fig 6B). The equation of linear regression is I (uA) = -133.678logC-23.589 (R^2=0.994). Where I represent peak current and microRNA represents microRNA concentration. More significantly, when the SNR is 3(where is the standard deviation of a blank solution, n=11), the detection limit was estimated to be as low as 21 aM. Therefore, compared to those reported by most of the microRNA biosensors, this method has a short manufacture the biosensor and to perform the determination time, ideal detection linear range, and compared with other detection methods, its actual detection limit (LOD) is reduced by an order of magnitude, exhibited satisfying performance for microRNA detection with improved (Table 1).

3.6 Selectivity, reproducibility and stability of the biosensor

The as-proposed microRNA biosensor also has high selectivity. To explore the specificity of our proposed microRNA biosensor, we conducted a comparative study of perfectly complementary, single-base mismatch microRNA-21 and non-complementary target microRNA at a concentration of 100 fM, 500 fM, 500 fM respectively, and the corresponding SWV signals were collected in Fig 7A. Compared with all biosensors, the oxidation peak current corresponding to the expected target microRNA-21 was lower than that of the other mismatched targets, indicating that our proposed biosensor has good selectivity. The excellent selectivity of this microRNA biosensor can be ascribed to the specific affinity of ssRNA to microRNA.

In addition to, reproducibility of the microRNA biosensor, another analytical parameter was also investigated. The shown in Fig 7B, each electrode surface was modified with the same complex (ssRNA-Cd^{2+}-CQDs-AMNFs) to detect the same concentration of microRNA-21 under the same experimental conditions. At a concentration of 10 fM, the relative standard deviation (RSD) of the sensor is 2.6%, indicating good repeatability.

As shown in Fig 7C, no obvious signal change is observed after 12 days, of which the signal remains ca. 101.2% of the original signal, also revealing the good stability of based ssRNA-Cd^{2+}-CQDs-AMNFs biosensor at a concentration of 100 fM.

3.7 Analytical application of the proposed microRNA biosensor

To further investigate the suitability of the proposed microRNA biosensor in serum, we added microRNAs at concentrations of 0 aM - 100 pM in normal human serum samples and operated according to the above standard method. Table 2 shown the electrochemical analytical results for microRNA-21. It can be seen that the recoveries were between 92.1% and 98.2%, and the relative standard deviation was less than 5.20%, demonstrating the promising utilization potentiality of the microRNA biosensor in real biological samples.

4. Conclusions

In this paper, we have successfully developed an ultrasensitive of AMNFs based electrochemical biosensor in the quantitative detection of breast cancer-associated microRNA-21.

The metal ions with high signal amplification ability were applied to microRNA biosensors, which exhibited significantly oxidation peak current activities than other signals. The CQDs due to their strong electrical conductivity and large specific surface era were employed as a substrate to the metal ion. The AMNFs-CQDs-metal ion-based microRNA-21 biosensor has a limit of detection is 21 aM, Based on the direct detection and quantification of microRNA-21 levels, it represents the highest sensitivity of microRNA-21 detection to date. More importantly, the signal changed due to the special interaction between antiomene and ssRNA and dsRNA. Therefore, the proposed electrochemical microRNA biosensor is the first reported method for related nucleic acid detection using antimonide materials and provides a rare opportunity for the development of electrochemical sensors. Finally, our proposed electrochemical microRNA biosensor opens up a new method for the determination of microRNA-21, as shown above, is also applied to the detection of other relevant tumor markers

Acknowledgments

This work was supported by the National Natural Science Foundation of China

(NO.81772290 and 81271930), Graduate Scientific Research and Innovation Foundation of Chongqing, China (2020CDCGJ014 ， CYS20076) ， Fundamental Research Funds for the Central Universities （ 2019CDYGZD007).The Higher Education Teaching Reform Research Project of Chongqing(203249).

References

[1]Yi W, Cai R, Xiang D,A novel photoelectrochemical strategy based on an integrative photoactive heterojunction nanomaterial and a redox cycling amplification system for ultrasensitive determination of microRNA in cells. Biosensors and Bioelectronics 143(2019):111614-.https://doi.org/10.1016/j.bios.2019.111614.

[2]Su S, Hao Q, Yan Z,A molybdenum disulfide@Methylene Blue nanohybrid for electrochemical determination of microRNA-21, dopamine and uric acid.. Microchimica Acta,186(2019).https://doi.org/10.1007/s00604-019-3678-0

[3].Cheng H, Li W, Duan S , Mesoporous Silica Containers and Programmed Catalytic Hairpin Assembly/Hybridization Chain Reaction Based Electrochemical Sensing Platform for MicroRNA Ultrasensitive Detection with Low Background. Anal Chem,91(2019):10672-10678.https://doi.org/10.1021/acs.analchem.9b01947.

[4]Zhang C, Wen K,Yang X,Rolling circle amplification-mediated in situ synthesis of palladium nanoparticles for the ultrasensitive electrochemical detection of microRNA. Analyst ,144(2019):3817-3825.https://doi.org/10.1039/C9AN00427K.

[5]Guo WJ, Wu Z, Yang XY,Ultrasensitive electrochemical detection of microRNA-21 with wide linear dynamic range based on dual signal amplification. Biosens Bioelectron ,131(2019):267–273.https://doi.org/10.1016/j.bios.2019.02.026.

[6]Jin, Wang, Jian,An ultrasensitive electrochemical biosensor for detection of microRNA-21 based on redox reaction of ascorbic acid/iodine and duplex-specic nuclease assisted target recycling. Biosens Bioelectron,9(2019):16-24.https://doi.org/10.1016/j.bios.2019.01.031.

[7] Bharti A, Agnihotri N, Prabhakar N,A voltammetric hybridization assay for microRNA-21 using carboxylated graphene oxide decorated with gold-platinum bimetallic nanoparticles. Microchim Acta,18(2019):185-193.https://doi.org/10.1007/s00604-019-3302-3.

[8] Ghazizadeh E, Naseri Z, Jaafari MR,A fires novel report of exosomal electrochemical sensor for sensing micro RNAs by using multi covalent attachment p19 with high sensitivity. Biosens Bioelectron,146(2018):74-81.https://doi.org/10.1016/j.bios.2018.04.023.

[9]Tian L, Qi J, Oderinde O,Planar intercalated Copper (II) complex molecule as small molecule enzyme mimic combined with Fe3O4 nanozyme for bienzyme synergistic catalysis applied to the microRNA biosensor. Biosens Bioelectron,142(2018): 110-117.https://doi.org/10.1016/j.bios.2018.03.045.

[10] Kangkamano T, Numnuam A, Limbut W,Pyrrolidinyl PNA polypyrrole/silver nanofoam electrode as a novel label-free electrochemical miRNA-21 biosensor. Biosens Bioelectron,145(2017):217-225.

https://doi.org/10.1016/j.bios.2017.11.024.
[11] Bo B, Zhang T, Jiang Y,Triple Signal Amplification Strategy for Ultrasensitive Determination of miRNA Based on Duplex Specific Nuclease and Bridge DNA–Gold Nanoparticles. Anal Chem,90(2018):2395-2400.
https://doi.org/10.1021/acs.analchem.7b05447.
[12] Feng KJ, Jin L, Lei D,Amperometric detection of microRNA based on DNA-controlled current of a molybdophosphate redox probe and amplification via hybridization chain reaction. Microchimica Acta,185(2018):28.
https://doi.org/10.1007/s00604-017-2579-3.
[13] Yuan YH, Wu YD, Chi BZ,Simultaneously electrochemical detection of microRNAs based on multifunctional magnetic nanoparticles probe coupling with hybridization chain reaction. Biosens Bioelectron ,234(2017):325-342.
https://doi.org/10.1016/j.bios.2017.06.022.
[14] Liu, Wei, Lu,Dual-mode electrochemical analysis of microRNA-21 using gold nanoparticle-decorated MoS2 nanosheet. Biosens Bioelectron,94(2017):552-229.
https://doi.org/10.1016/j.bios.2017.03.040.
[15] Wang Z, Zhang R, Zhao M,High-Yield Production of Stable Antimonene Quantum Sheets for Highly Efficient Organic Photovoltaics. J Mater Chem A, 123(2018):245-255.https://doi.org/10.1039/c8ta07214k.
[16]Yu J, Hong WX, Feng J,Antimonene Nanoflakes: Extraordinary Photoacoustic Performance for High-Contrast Imaging of Small Volume Tumors. Adv Healthc Mater ,17(2019): 345-355.https://doi.org/10.1002/adhm.201900378.
[17] He J, Zhang F, Xiang Y,Preparation of low dimensional antimonene oxides and their application in Cu:NiO_x based planar p-i-n perovskite solar cells. J power Sources,435 (2019): 981–987.https://doi.org/10.1016/j.jpowsour.2019.226819.
[18] Zhang C, Li Y, Zhang P,Antimonene quantum dot-based solid-state solar cells with enhanced performance and high stability. Sol Energ Mat Sol Cell 89(2019): 11-20.https://doi.org/10.1016/j.solmat.2018.09.007.
[19] Yu J, Xiu HW, Feng J,Antimonene Nanoflakes: Extraordinary Photoacoustic Performance for High-Contrast Imaging of Small Volume Tumors. Adv Healthc Mater,8(2019):1900378. https://doi.org/10.1002/adhm.201900378.
[20] Chen M, Gan N, Zhou Y,A novel aptamer- metal ions- nanoscale MOF based electrochemical biocodes for multiple antibiotics detection and signal amplification. Sens Actuators B Chem,242(2017):1201-1209.https://doi.org/10.1016/j.snb.2016.08.185.
[21] Wu KY, Chen M, Huang NH,Facile and recyclable dopamine sensing by a label-free terbium(III) metal-organic framework. Talanta ,221(2020):99-102.https://doi.org/10.1016/j.talanta.2020.121399.
[22] Zhang DS, Yan PZ, Li YF,Atomically Thin Arsenene and Antimonene: Semimetal–Semiconductor and Indirect–Direct Band-Gap Transitions.Angewandte Chemie-International Edition,54(2015):3112-3115.https://doi.org/10.1002/anie.201411246
[23] Yu J, Wang XH, Feng J,Antimonene Nanoflakes: Extraordinary Photoacoustic Performance for High-Contrast Imaging of Small Volume Tumors. Adv Healthc

Mater,8(2019):1900378. https://doi.org/10.1002/adhm.201900378.
[24]He J, Zhang F, Xiang Y,Preparation of low dimensional antimonene oxides and their application in Cu:NiO_x based planar p-i-n perovskite solar cells, J power Sources 435(2019):226819.https://doi.org/10.1016/j.jpowsour.2019.226819.
[25] Zhang C, Li Y, Zhang P,Antimonene quantum dot-based solid-state solar cells with enhanced performance and high stability. Sol Energ Mat Sol C,189(2019):11-20.https://doi.org/10.1016/j.solmat.2018.09.007.
[26] Yu J, Xiu H W, Feng J,Antimonene Nanoflakes: Extraordinary Photoacoustic Performance for High-Contrast Imaging of Small Volume Tumors. Adv Healthc Mater,8(2019):1900378. https://doi.org/10.1002/adhm.201900378.
[27] Zhuang Q, Cao W, Ni Y,Synthesis-identification integration: One-pot hydrothermal preparation of fluorescent nitrogen-doped carbon nanodots for differentiating nucleobases with the aid of multivariate chemometrics analysis. Talanta,185(2018): 491-498.https://doi.org/10.1016/j.talanta.2018.04.019.
[28] Takemura K, Chowdhury AD, Park EY,Electrical pulse-induced electrochemical biosensor for hepatitis E virus detection. Nat Commun,10(2019):3737.https://doi.org/10.1038/s41467-019-11644-5.
[29] Tavallaie R, Darwish N, Gebala M,The Effect of Interfacial Design on the Electrochemical Detection of DNA and MicroRNA Using Methylene Blue at Low-Density DNA Films. Chem Electro Chem,1(2014):165-171. https://doi.org/10.1002/celc.201300136.
[30] X.M. Miao, W.H. Wang, T.S. Kang, J.B. Liu, K.-K. Shiu, C.-H. Leung, D.-L. Ma ,Ultrasensitive electrochemical detection of miRNA-21 by using an iridium(III) complex as catalyst. Biosens Bioelectron,86(2016):454-458.https://doi.org/10.1016/j.bios.2016.07.001.
[31] Liu, L., Xia, N., Liu, H.P., Kang, X.J., Liu, X.S., Xue, C., He, X.L., Highly sensitive and label-free electrochemical detection of microRNAs based on triple signal amplification of multifunctional gold nanoparticles, enzymes and redox-cycling reaction. Biosensors & Bioelectronics 53(2014):399-405.https://doi.org/10.1016/j.bios.2013.10.026.
[32] Yu, N. , Wang, Z. , Wang, C. , Han, J. , & Bu, H.,Combining padlock exponential rolling circle amplification with cofe2o4 magnetic nanoparticles for microrna detection by nanoelectrocatalysis without a substrate. Analytica Chimica Acta,962(2017):24-31.https://doi.org/10.1016/j.aca.2017.01.069.
[33]Shuai, H. L. , Huang, K. J. , Chen, Y. X. , Fang, L. X. , & Jia, M. P.,Au nanoparticles/hollow molybdenum disulfide microcubes based biosensor for microrna-21 detection coupled with duplex-specific nuclease and enzyme signal amplification.Biosens Bioelectron, 89(2017):989-997.https://doi.org/10.1016/j.bios.2016.10.051.
[34] Liang T, Kun Q, Jinxu Q, Qinyao L, Chen Y, Wei S, Yihong W,Gold nanoparticles superlattices assembly for electrochemical biosensor detection of MicroRNA-21. Biosens Bioelectron 99(2017):564-570.https://doi.org/10.1016/j.bios.2017.08.035.
[35]Bingchen L,Fei L,Yuanyuan P,Yunlei Z,Wenxuan F,Huanshun Y,Shiyun A, et

al.,Two-stage cyclic enzymatic amplification method for ultrasensitive electrochemical assay of microRNA-21 in the blood serum of gastric cancer patients. Biosens Bioelectron79(2016):307-312.https://doi.org/10.1016/j.bios.2015.12.051.

Figures and table captions

Scheme 1. MicroRNA biosensor schematic diagram and detection principle.

Figure 1. (A) TEM image of AMNFs; (B) TEM image of CQDs; (C) The AFM of AMNFs.

Figure 2. (A) The XRD spectra of AMNFs; (B) The FT-IR spectra of the CQDs; (C) The full-scan XPS spectra of CQDs-Cd; (D) the high-resolution XPS spectra of Cd3d; (E) the high-resolution XPS spectra of C; (F) the high-resolution XPS spectra of O.

Figure 3. SWV curves of signal tracers: (a) the ssRNA-Cd^{2+}-CQDs-AMNFs/GCE, (b) microRNA-21/ssRNA-Cd^{2+}-CQDs-AMNFs/GCE.

Figure 4. Cyclic voltammetry (CV) (A) and Electrochemical impedance spectroscopy (EIS) (B) of bare GCE (a), AMNFs/GCE (b), ssRNA-Cd^{2+}-CQDs-AMNFs/GCE (c), micro-RNA/ssRNA-Cd^{2+}-CQDs-AMNFs/GCE (d) in 5.0 $mmoL^{-1}$ $Fe(CN)_6^{4-/3-}$ containing 0.1 moL^{-1} KCl at 100 mVs^{-1}.

Figure 5. Optimization of the experimental parameters: (A): effects of incubation time on ssRNA-Cd^{2+}-CQDs/AMNFs/GCE incubated within 40 fM miRNA-21 solution in different recorded by SWV. (B) the adsorption density of antimony on ssRNA-Cd^{2+}-CQDs. Error bars=RSD (n=5).

Figure 6. (A) Typical SWV signals from microRNA-21-ssRNA-Cd^{2+}-CQDs-AMNFs/GCE fabricated microRNA biosensor after capturing various microRNA-21 concentrations (from (a) to h: 0 M, 100 aM , 1 fM, 10 fM, 100 fM, 1 pM, 10 pM, 100 pM and 1 nM). (B) The resulting calibration curves of the peak currents vs. Logarithmic microRNA-21 concentrations. Error bars=RSD (n=5).

Table 1. Comparison with the analytical characteristics of electrochemical biosensors reported for the determination of miRNAs in serum.

Figure 7. (A) SWV signals of the proposed microRNA biosensor are specific to the complementary target microRNA-21, the concentrations were 50 fM respectively. (B) independently fabricated 5 biosensors. (C) Stability of the electrochemical biosensor

for detecting microRNA-21 (100 fM) within 12 days. The electrochemical SWV response of same microRNA biosensors for five times.

Table 2. Determination of microRNA-21 added in human serum (n=5) with the biosensor.

Journal Pre-proofs

Scheme 1.

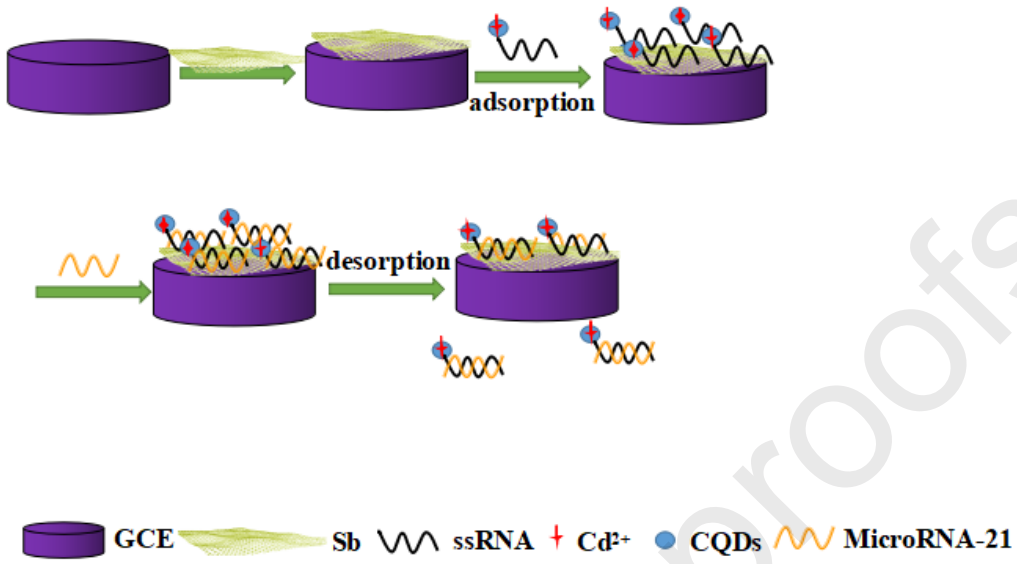

Journal Pre-proofs

Figure 1.

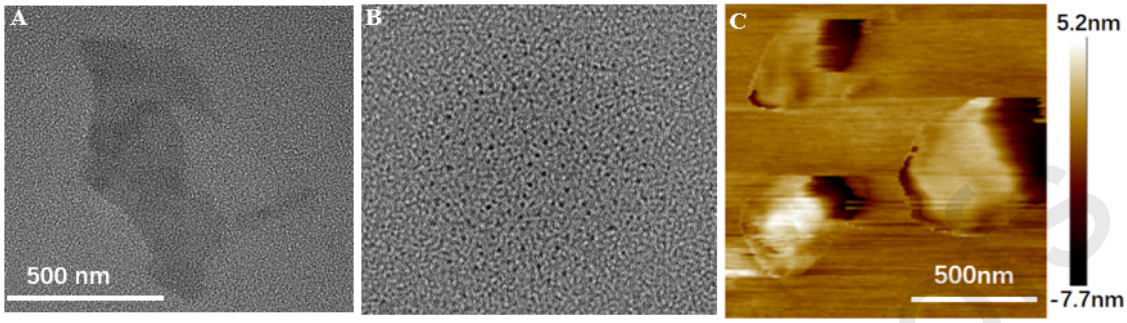

Figure 2.

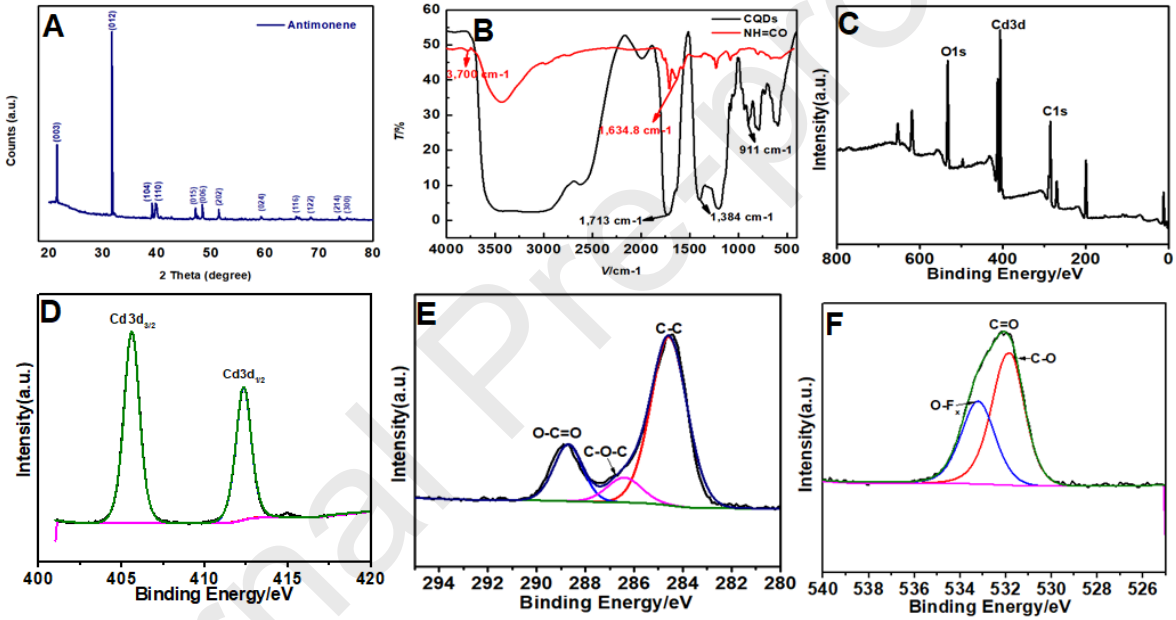

Journal Pre-proofs

Figure 3.

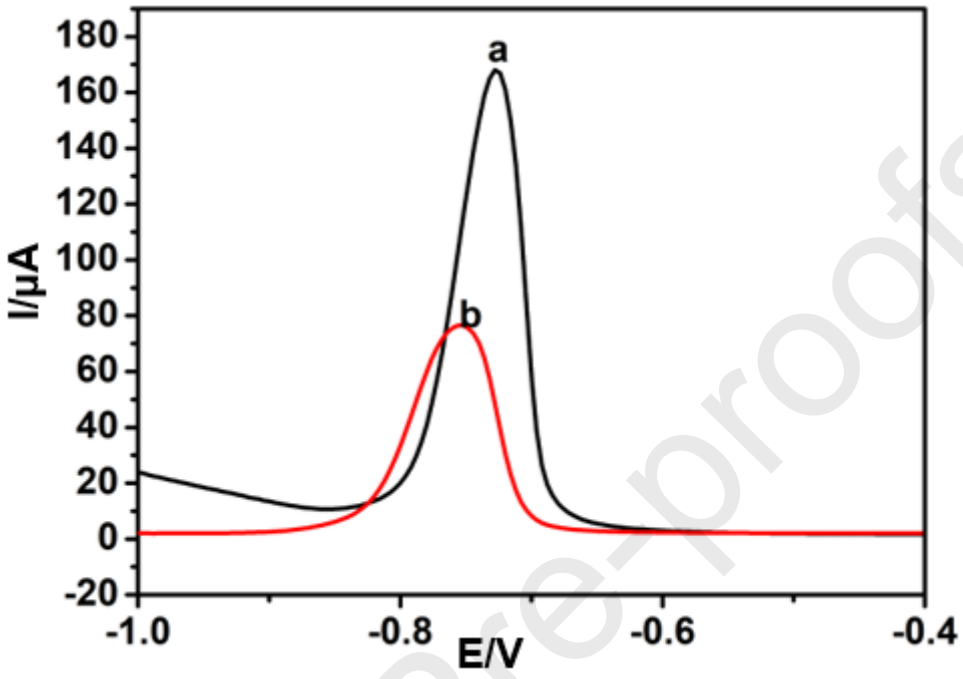

Journal Pre-proofs

Figure 4.

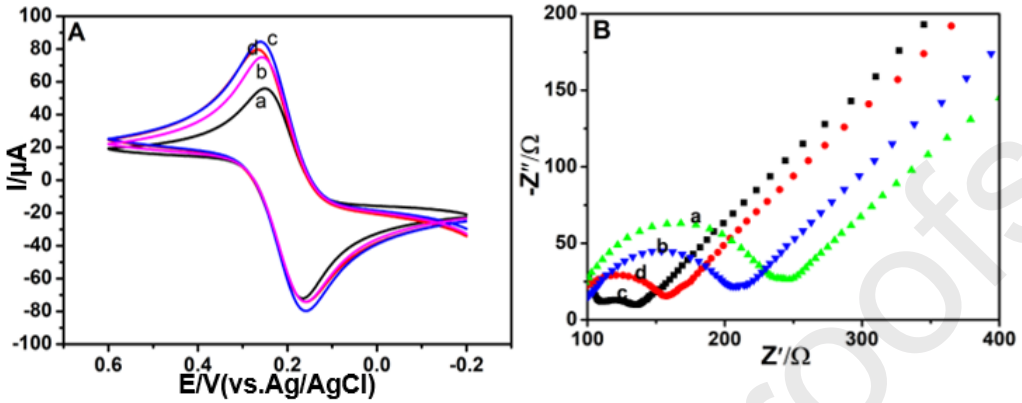

Figure 5.

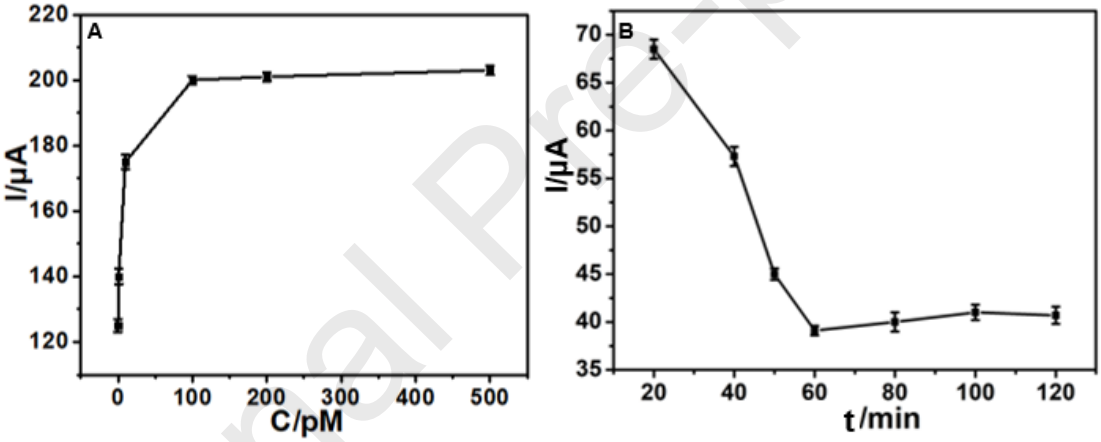

Journal Pre-proofs

Figure 6.

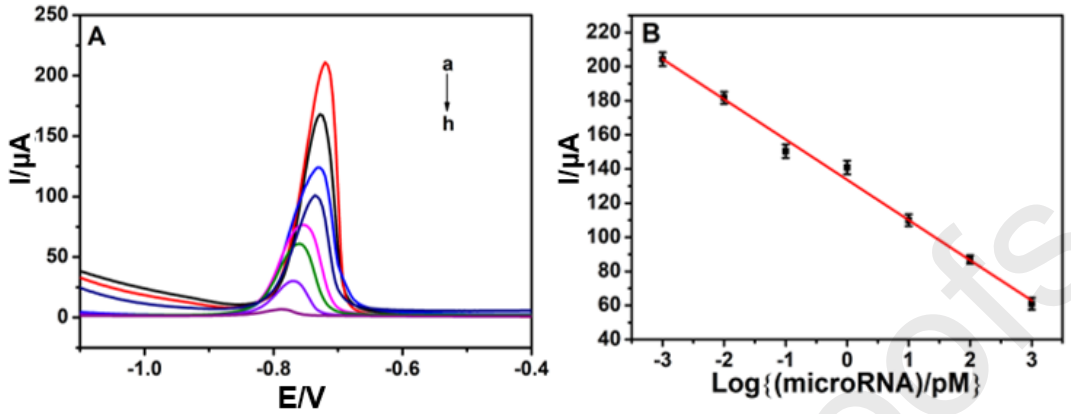

Journal Pre-proofs

Table 1.

Target microRNA	Method of signal amplification	Electrode/Electrochemical methods	Linear range	Detection limit	Time	References
microRNA-21	Hairpin capture probe/target recycling/MB	AuE/DPV	0.5 pM-2000 pM	56 fM	285 min	[29]
microRNA-21	MCH/Ir(III) complex	AuE/CV	5 fM-1 pM	1.6 fM	1125 min	[30]
microRNA-21	AuNPs/SA-ALP/redox cycling	AuE/Amp	10 fM-5 pM	3 fM	825 min	[31]
microRNA-21	Au@CoFe2O4/Tb-Gra/rolling circle amplification	GCE/SWV	1 fM−2 nM	0.3 fM	600 min	[32]
microRNA-21	MoS2/AuNPs/SA-ALP	GCE/DPV	0.1 fM−0.1 pM	0.086 fM	900 min	[33]
microRNA-21	AuNS/capture probe/TB	GCE/DPV	100 aM-1 nM	78 aM	210 min	[34]
microRNA-21	AuNPs/capture probe/redox cycling	AuE/DPV	1 fM-100 pM	0.36 fM	200 min	[35]
microRNA-21	Cd^{2+}-carbon quantum dots-ssRNA-antiomene	GCE/ SWV	100 aM-100 nM	21 aM	150 min	This work

Journal Pre-proofs

Figure 7.

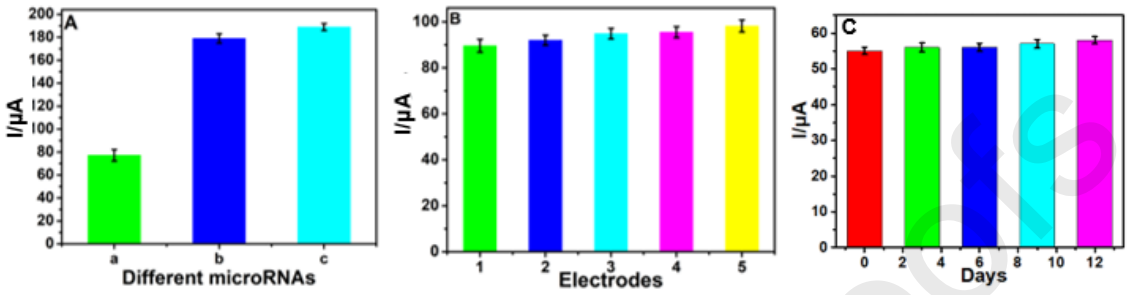

Table 2.

Addition s of Sample	Standard value/μA	Found value/μA	Recovery (%)	RSD (%)
0	0.8	2.6	-	-
100 pM	167	168	98.3	2.56
60 pM	76.5	79	92.5	3.68
100 fM	57.2	61	98.2	1.89
40 fM	56.6	57.5	96.1	2.56
20 aM	22.9	25.9	97.6	3.28

Journal Pre-proofs

Declaration of interests

The authors declare that they have no known competing financial interests or personal relationships that could have appeared to influence the work reported in this paper.

Journal Pre-proofs